Magnetic microelastography for evaluation of ultrasound-induced softening of pancreatic cancer spheroids

G. Laloy-Borgna, L. Vovard, A. Rohfritsch, L. Wang, J. Ngo, M. Perier, A. Drainville, F. Prat, M. Lafond, C. Lafon, et al.

Magnetic micro-elastography for evaluation of ultrasound-induced softening of pancreatic cancer spheroids

G. Laloy-Borgna[1] L. Vovard[1] A. Rohfritsch[1] L. Wang[1] J. Ngo[1]
M. Perier[1] A. Drainville[1] F. Prat[2] M. Lafond[1] C. Lafon[1]
S. Catheline[1]

[1]LabTAU, INSERM, Centre Léon Bérard, Université Lyon 1, F-69003, LYON, France
[2]Institut Cochin, INSERM, PARIS, France

Abstract

Pancreatic ductal adenocarcinoma (PDAC) is a devastating disease with very low survival rates 5 years after diagnosis. The main reason for this dismal prognosis is the thick stroma which both protects tumor cells from drug penetration and supports tumor development. Ultrasound inertial cavitation is a promising treatment with a potential for stromal disruption, enhancing tumor cells sensitivity to chemical agents and biomodulators. Our goal was to develop a dedicated micro-elastography setup allowing to measure the elasticity of *in vitro* tumor models called spheroids. In a second step, the impact of cavitation treatment on their mechanical properties was assessed.

A transcranial magnetic stimulation (TMS) clinical device was used to induce shear waves in the spheroids containing magnetic nanoparticles. Using an inverted optical microscope, Particle Imaging Velocimetry (PIV) and noise correlation algorithms, the shear wave velocity, indicative of the medium's elasticity, could be measured.

Shear waves generated by the magnetic pulse inside the spheroids were detected and their velocity was measured using noise correlation elastography. This allowed the estimation of the spheroids elasticity. Cavitation treatment softened them significantly, the impact of the exposure conditions and the spheroids composition have been studied. In the future, such a method could be used to monitor cavitation treatments.

In addition, since it is now well established that mechanical constraints and elasticity play an important role in tumor growth, it is of high interest to measure the elasticity of tumor models to better understand the mechanisms of tumor growth.

INTRODUCTION

The pancreas is a vital organ, secreting a number of substances essential to food digestion and blood sugar regulation such as insulin, glucagon, and the pancreatic juice (containing bicarbonate and digestive enzymes among others). Among the pathologies that can affect the pancreas, the most common pancreatic cancer is called pancreatic ductal adenocarcinoma. It is a devastating disease, since the survival rate of patients 5 years after diagnosis is less than $10\,\%$ and the incidence of this type of cancer is around 500 000 per year worldwide [1]. It is anticipated to become the second cause of cancer-related death in the USA by 2030 [2]. The only existing curative option for this type of cancer is surgery, but this is rarely possible [3]. Hence radiotherapy and chemotherapy are currently the most used treatments, even if they are only adjuvant treatments that may potentially downstage the tumor and make it resectable. However, the effectiveness of chemotherapy on this type of tumor is low, due to a thick, predominant stroma (which represents

around $80\,\%$ of the tumor mass [4]). It protects tumor cells from external damage, prevents the penetration of drugs, and promotes tumor development [4].

One of the therapeutic avenues currently being explored for this type of cancer is this stroma, which is targeted to improve the efficacy of chemotherapy. Ultrasound is one of the methods that can be used to reshape or loosen the stroma and improve the tumor response to chemical agents [5, 6]. The therapeutic strategy proposed as part of our project involves the use of inertial ultrasound cavitation to enhance drug delivery to pancreatic tumors, potentially improving their therapeutic response. Ultrasound cavitation refers to the formation and collapse of air bubbles in a biological tissue due to high intensity focused ultrasound. The improved penetration and efficacy of drugs on tumor models after exposure to ultrasonic cavitation has already been demonstrated *in vitro* [7], but the application to clinics requires further development. The starting hypothesis is that the application of an inertial cavitation sequence without injecting any nucleation agents must be applied beforehand to degrade collagen fibers and alter the tumor micro-environment to increase the penetration of treatments. The mechanisms by which cavitation could alter the tumor and enhance drug penetration could include: increasing tumor permeability through increased extravasation, softening the tumor mass through decreased interstitial pressure, or activating a specific immune response within the tumor.

The aim of the present work was to develop a method allowing to estimate the elasticity of spheroids, in order to understand better the impact of the cavitation treatment on their mechanical properties. Hence we propose hereafter an optical micro-elastography experiment allowing to estimate the spheroids elasticity thanks to the study of shear wave propagation. Various methods have already been developed for measuring the elasticity of spheroids. Among the static methods, optical coherent elastography [8], micro-clamps [9] or atomic force microscopy [10] have been applied. Among the dynamic methods, on the one hand Brillouin light scattering microscopy [11] allows to measure the compression elastic modulus of spheroids and on the other hand, completely passive micro-elastography (taking advantage of ambient vibrations) was used to characterize millimeter-sized tissue engineering samples [12]. However, these methods present some drawbacks such as the measurement duration compared to biological processes, or their failure in retrieving a quantitative elastic modulus.

In this article, we present first the developed method allowing to induce elastic waves in the tumor models using a magnetic pulse and to further retrieve the local shear wave velocity. Next, a control experiment involving incubation in trypsin is presented to determine which mechanical parameter the measurement is sensitive to. Finally, the impact of a cavitation treatment on the mechanical properties of spheroids is evaluated.

MATERIALS AND METHODS

1 - Spheroids fabrication

The spheroids were produced using a kit marketed by Greiner™(Kit M3D Nanoshuttle-PL #657841, Greiner Bio-One, Kremsmünster, Austria). The spheroids consisted of two independently cultured cell lines, named KPC A219 and iMEF, respectively. KPC A219 is a pancreatic cancer cell line derived from transgenic mice with two mutations: Kras and p53. iMEFs (Immortalized Mouse Embryonic Fibroblasts) are non-cancerous fibroblasts which, among other things, form the stroma in a real pancreatic tumor, and were therefore used here to model this stroma. These two cell lines were provided by Julie Guillermet-Guibert from Centre de Recherches en Cancérologie in Toulouse. They were cultured at $37\,^{\circ}\mathrm{C}$, 5% of CO_2, in DMEM/F12 (Gibco 11530566, Thermo Fisher Scientific, Waltham, Massachusetts, USA), supplemented with 10% SVF (Gibco 10270106), 100 U/mL of penicillin and 100 μg/mL of streptomycin (Gibco 15140122), and L-glutamin (Gibco 25030024).

The protocol used to manufacture spheroids is as follows: three days before the elastography experiment, a cell passage was performed, the cells

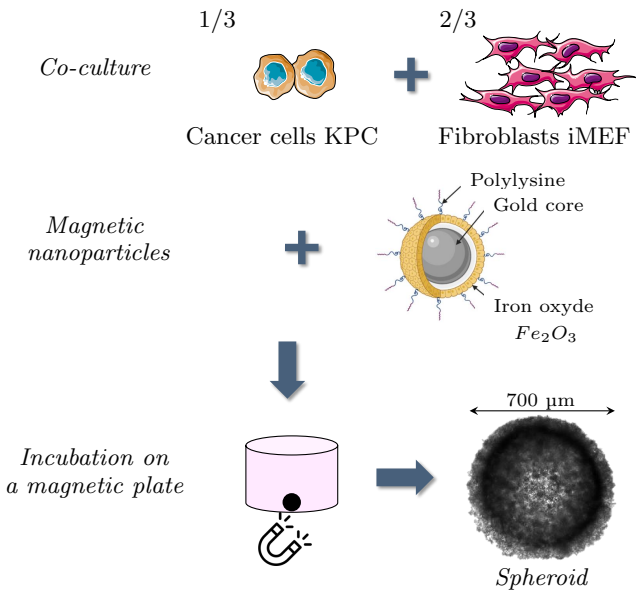

Figure 1: Experimental protocol used to obtain magnetic tumor models called spheroids.

were counted and distributed among several flasks. Two days later, TGFβ (Peprotech 100-21, Cranbury, USA) was added to the flask containing the iMEFs, a growth factor that activates fibroblasts and triggers the desmoplastic fibrous reaction, corresponding to excessive production of fibrous tissue and activation of the cellular components of the stroma. Nanoshuttles were also added to the cells. These are magnetic nanoparticles made of gold nanoparticles within which Fe_2O_3 is placed, functionalized by Poly-L-Lysine, a cell-binding amino acid polymer. Nanoshuttles were incubated with cells for 24 hours, allowing them to bind to the cells. Finally, on the day of spheroid formation, 10 000 KPC and 20 000 iMEF were placed in each well of a 96-well cell culture plate (cell-repellent plates, Greiner 655970), and the plate was placed on top of a 96-magnet plate. The magnets allowed all the functionalized cells to be concentrated in a single point above the magnet, thus promoting the creation of inter-cellular bonds and ultimately the formation of a spheroid. The schematic protocol and the morphology of spheroids after 6 h of incubation are shown in figure 1. In addition, the evolution of the spheroids morphology along time can be seen in figure 11 in Supplementary Material A. Biological tests, such as viability measurements, were generally carried out 4 days later, but for elastography the experiments were carried out six hours after the spheroids had begun to form, so that they would have some transparency for image processing.

2 - Experimental setup for micro-elastography

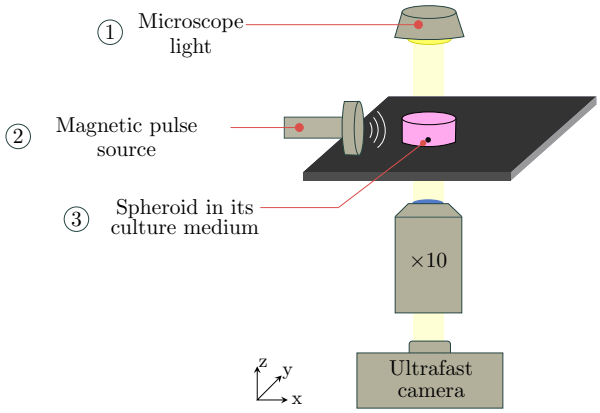

(a) Scheme

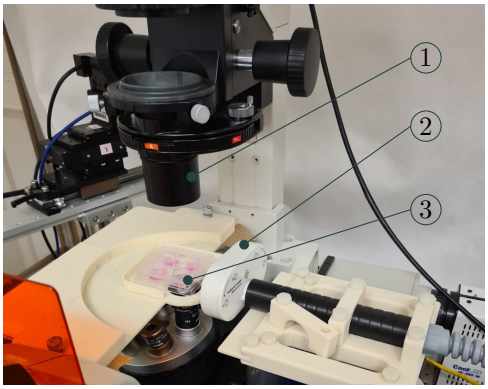

(b) Picture

Figure 2: Experimental setup used to generate a pulsed magnetic field to induce elastic waves in a spheroid. (a) Scheme and (b) picture of the experimental setup.

The experimental setup was composed of an ultrafast camera (Phantom v12.1, Wayne, New Jersey,

USA), an inverted microscope (Nikon Ti-S, Tokyo, Japan) and a clinical transcranial magnetic stimulation device (Mag&More, München, Germany). The ultrafast camera was plugged directly onto the microscope, and acquired 512x512 127 ms videos, at a frame rate of 21 000 Hz. A $10\times$ magnification lens was used. A 4-well culture plate was used and a spheroid was placed in each well with $500\,\mu L$ of $37\,^{\circ}C$ culture medium (complete DMEM). The imaging plane was chosen to be approximately in the center of the spheroid. The magnetic stimulator was placed so that the magnetic field peak was positioned on the studied spheroid. The camera was triggered so that the magnetic pulse occurred 2.3 ms after the beginning of the video acquisition. The corresponding experimental setup is presented in figure 2. Prior to the experiments on spheroids, experiments were carried out on in-house phantoms to prove the feasibility of such an experiment. The results are presented in the supplementary material B.

3 - Data processing for elastography measurements

Particle velocity field computation In a first step, the particular velocity field was retrieved from the images acquired with the camera. In this case, Particle Imaging Velocimetry (PIV) algorithms used in fluid mechanics were used. A Matlab toolbox called PIVlab [13] was employed with three iteration steps with squares of 32, 16 and 8 pixels sides. Additionally, a band-pass frequency filter was applied to the velocity field, with 1 and 5 kHz as cutoff frequencies.

Wave velocity measurement using noise correlation elastography In order to measure the wave speed inside the propagation medium, indicative of its elasticity, noise correlation algorithms [14–17] were applied to the filtered wave field. Based on time reversal and originally developed for passive elastography, the local wave speed in a medium can be estimated by computing the time-reversed wave field and its derivatives at each point of the imaged medium.

It was previously demonstrated that the local wave velocity v_s, defined by the ratio of the pulsation ω and the wave vector k can be estimated through the time-reversed particle velocity field V^{TR} and the time reversed strain field ξ^{TR}:

$$v_s = \frac{\omega}{k} \cong \sqrt{\frac{V^{TR}}{\xi^{TR}}} \tag{1}$$

with $V^{TR} = \frac{\partial \phi}{\partial t}(-t) \otimes \frac{\partial \phi}{\partial t}(t)$ and $\xi^{TR} = \frac{\partial \phi}{\partial r}(-t) \otimes \frac{\partial \phi}{\partial r}(t)$ where $\otimes_t$ represents the time convolution product, ϕ the particle velocity field, t the time coordinate and r the spatial coordinate.

The application of the above equations allows to get shear wave velocity maps indicating the local elasticity inside the spheroids.

4 - Trypsin experiment

An experiment consisting in comparing the shear wave velocity inside the spheroids before and after an incubation in trypsin is presented hereafter. It is known that incubation of spheroids in trypsin destroys inter-cellular bonds and thus dissociates the spheroids [7]. The use of this enzyme in elastography experiments makes it possible to test the effect of the weakening of inter-cellular bonds on the measurement. The protocol used for this test is as follows: an elastography acquisition is first performed on a 6 h-old spheroid placed in its culture medium. The spheroid is then extracted from its culture medium and placed in a trypsin solution at $37\,^{\circ}C$ concentrated to $0.25\,\%$ (Gibco ™ 25200056) for 30 minutes. The spheroid is then extracted from the trypsin and returned to its culture medium, where a second elastography acquisition is performed. The incubation time in trypsin was optimized to ensure that trypsin had an effect on the spheroid, but that it still appeared to have some cohesion and was not completely dissociated.

5 - Application of cavitation treatment

Without the presence of exogeneous nuclei such as echocontrast agents, ultrasonic cavitation can occur through activation of dissolved gas pockets [18].

Our device takes advantage of long, moderate intensity pulses and the confocal geometry to nucleate cavitation from these gas nuclei already present within the spheroid or in the surrounding fluid [19–21]. It is composed of two confocally-positioned ultrasonic piezoelectric transducers with 50 mm diameter and 50 mm radius of curvature operating at a frequency of 1.1 MHz, with a hydrophone within the water tank to monitor acoustic cavitation signals from the focus. In order to position the spheroid precisely, an Eppendorf tube into which an Agar gel with a well had been poured (see figure 3, right-hand side) was placed on a tube holder, such that the lower half of the tube was immersed in water and the spheroid was at the focal point of the transducers.

The spheroid was then exposed to acoustic pulses with a 2750-cycle duration and a pulse repetition frequency of 250 Hz, producing a duty cycle of 12.5%. The focal pressure was dynamically varied between 3.1 and 5.1 MPa to achieve a predefined cavitation level. This pressure range was measured using a calibrated FOPH 2000 fiber optic hydrophone (RP Acoustics, Leutenback, Germany) accross the entire range of the amplification chain. A cavitation index (CI) was used, defined as the average of the frequency spectrum (in dB) obtained from the hydrophone from 0.1 to 7 MHz, relative to a reference level measured when no acoustic signal was present [20, 22]. CI values of either 20 or 26 were used for different groups with total treatment duration of either 20 or 60 seconds. While the corresponding pressure varied across samples, maintaining a constant CI of 20 or 26 dB necessitated pressures around 3 and 4.5 MPa, respectively.

6 - Statistical tests

The statistical analyses were conducted using the PRISM software (GraphPad Software, Insight Partners, New York City, USA). Data normality was assessed for each group of data using d'Agostino and Pearson tests. In the case of normality ($p>0.05$), ANOVA was performed, applying Bonferroni's multiple comparisons correction for the datasets requiring more than one test. For the only dataset failing the normality test (non-treated spheroids in figure 9 ; $p<0.05$), Friedman test with Dunn's multiple comparisons was performed. For the experiment with trypsin, a single T-test on paired data was used.

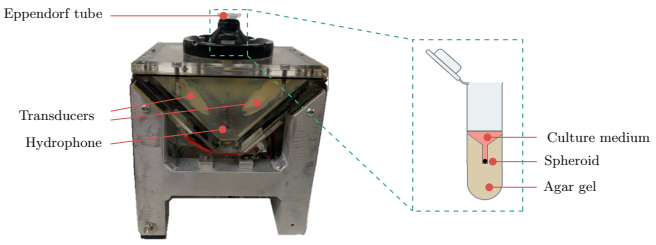

Figure 3: Device used to apply the cavitation treatment onto the spheroids. An Eppendorf tube partly filled with an Agar gel was used to locate the spheroid at a precise point corresponding to the focal point of the ultrasonic transducers.

RESULTS

1 - Elastography measurements

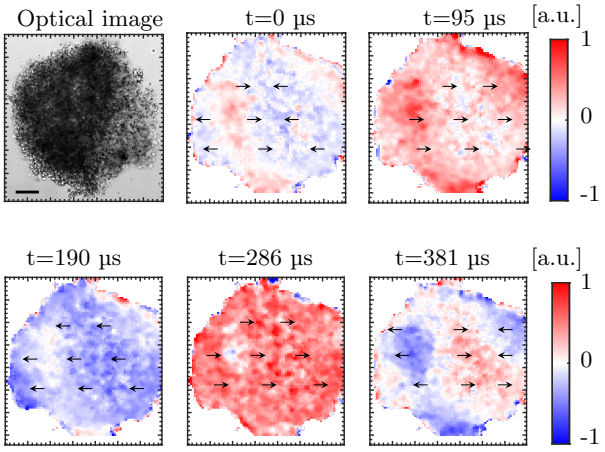

Figure 4: Snapshots of the X-component (see figure 2) of the particle velocity field. The raw optical image is presented on the left and the displacement field at different times are shown in red/blue colors. Scale bar=100 µm.

Elastic waves induced in the tumor models Instantaneous images of the particle velocity field

measured along the X-direction were coded in red and blue on a normalized scale (figure 4). We can see that positive and negative displacements alternate at different times, corresponding to an oscillation of the cells. In fact, whatever the direction in which the displacements were measured, the same type of behavior and displacement pattern was found.

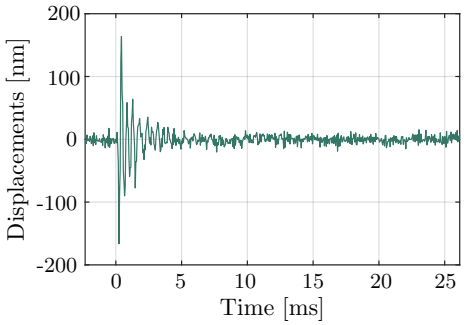

(a) Displacement temporal signal

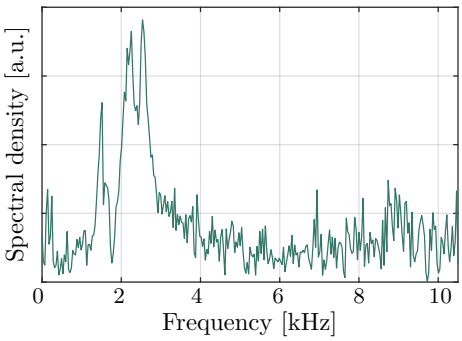

(b) Displacement spectrum

Figure 5: Displacement signal along time and its spectral density as a function of frequency.

More quantitatively, figure 5a shows a displacement signal averaged over a square of $10\times10\,\text{pixels}^2$ as a function of time. As expected, at time t=0 corresponding to the magnetic pulse, there is a very sharp increase of the measured displacements, clearly emerging from the background noise previously present. The maximum displacement amplitude between two frames is of 160 nm in this case, corresponding to $\frac{1}{12}^{th}$ of the pixel size. This displacement signal oscillates over time, with at least 10 periods of oscillation clearly visible. Next, the signal attenuates over time. The spectrum of this signal is plotted in figure 5b. It indicates that the displacement signal is broadband, since between 1 and $4\,\text{kHz}$ the amplitude of the Fourier transform is higher than the background noise.This displacement spectrum is the consequence of the whole motion generation chain, from the magnetic pulse to the displacements measured in the spheroids. Indeed, the magnetic pulse consists of a single sinusoidal cycle at a frequency of $5.8\,\text{kHz}$. It acts on the magnetic nanoparticles described as magnetic dipoles to align them on the external magnetic field. These dipoles don't align immediately on the magnetic field, due to their inertia, to the viscosity of the medium, as well as to the nature of the bonds between the particles and the cells. Overall, the physical phenomena generating elastic waves inside the spheroids from an external magnetic field behave as a low-pass filter, which is consistent with what is observed.

Measurement of the local wave velocity Three examples of wave velocity maps obtained using noise correlation elastography algorithms are shown in figure 6. On the one hand, the average velocities measured within the spheroids are mostly between 1 and $2\,\text{m}\,\text{s}^{-1}$. On the other hand, all three maps exhibit the same spatial distribution: a corona on the outside of the spheroid with higher wave velocities than at the center.

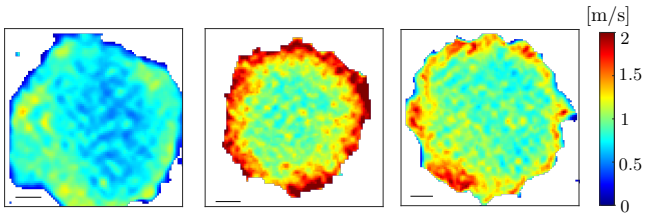

Figure 6: Examples of shear wave velocity maps obtained on three different spheroids. Scale bars=$100\,\mu\text{m}$.

In this first stage, waves were generated inside the spheroids with a magnetic pulse and shear wave velocity maps could be retrieved using noise correlation algorithms. However, in such a complex medium made of two types of cells and magnetic nanoparticles, the physical sense of the elasticity

probed by shear waves is not trivial. Nonetheless, since the wavelengths ($500\,\mu m$) are smaller than the spheroids but very large compared to the cells size (around $15\,\mu m$ of diameter), it is unlikely that the waves would be sensitive to the intrinsic cells elasticity but rather to the bonds strength. The following experiment using trypsin was used to elucidate this aspect.

2 - Influence of incubation in trypsin

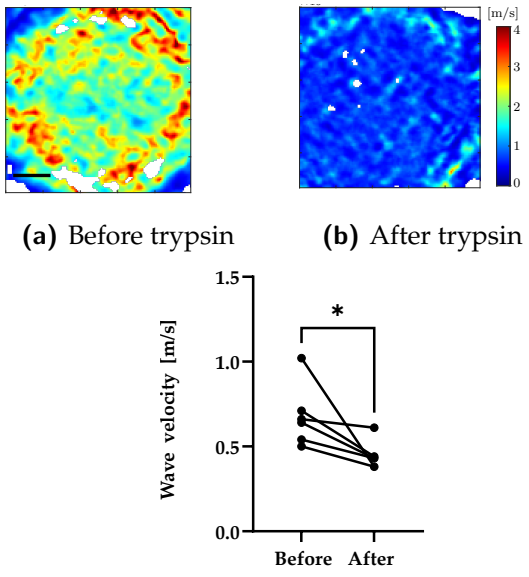

(a) Before trypsin **(b)** After trypsin

(c) Statistical test

Figure 7: Influence of trypsin on the wave velocity measured on spheroids. (a) Example of a wave velocity maps obtained on one spheroid before and (b) after incubation in trypsin. (c) Statistical analysis on six average velocity measurements[1]. A paired T-test was used in this case. Scale bar=$100\,\mu m$. * indicates $p < 0.05$.

The influence of the spheroid incubation in trypsin was studied and these results are shown in figure 7. Wave velocity maps obtained on the same spheroid before and after incubation in trypsin are presented, showing a sharp decrease in wave velocity. The experiment was carried out on three spheroids, giving six velocity measurements (one velocity map per displacement polarization), a statistical study is presented in figure 7c. For each spheroid, mean wave velocity was used as an observable, and one paired-data T-test was performed. The difference between mean velocities before and after incubation in trypsin was statistically significant, with a systematic decrease in velocity after incubation in trypsin. Hence this experiment allowed to conclude that the developed method is sensitive to the intercellular elasticity, since the effect of trypsin is statistically significant and induces a decrease in velocities.

3 - The cavitation treatment effect on the spheroids

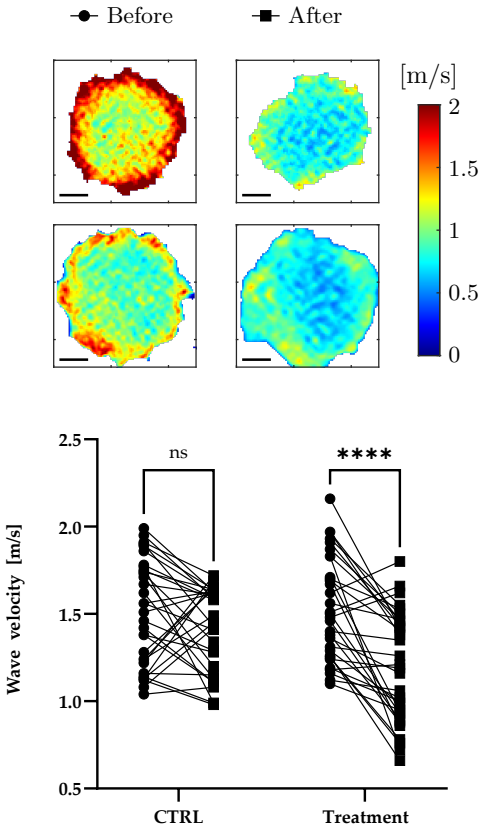

Figure 8: Effect of the cavitation treatment on average wave velocities measured within the spheroids. On the left are displayed two examples of wave velocity maps acquired before and after the cavitation treatment. On the right the statistical analysis result is shown, comparing one control group with one treated group. Scale bars=$100\,\mu m$. **** indicates $p < 0.0001$.

To evaluate the impact of the cavitation treatments on the spheroids mechanical properties, a control and a treated group were compared. For the control group, the spheroids were transferred to Eppendorf tubes and then put back again in the 4-well culture plates. Indeed, this pipetting operation could sometimes alter some spheroids and lead to a decrease in wave velocity.

Figure 8 shows the wave velocity of spheroids with nominal parameters (spheroids containing 2/3 iMEF and 1/3 KPC, exposed to a 26 dB cavitation treatment during 20 s). On the left, wave velocity maps obtained before and after the cavitation treatment are shown for two example spheroids. Wave velocities decreased overall for both spheroids. The statistical analysis compares the control and the treatment groups. On the one hand, for the control group, a non-significant decreasing trend was observed ($p = 0.211$). On the other hand, when a cavitation treatment was applied, mean velocities within spheroids decreased for most spheroids ($p<0.0001$), suggesting that the cavitation treatment significantly weakened inter-cellular bonds.

Influence of the treatment parameters In a second step, the influence of the treatment parameters was investigated. Indeed, if the significant decrease of the wave velocity due to cavitation was proved, one can wonder if the treatment parameters influence the mechanical impact and if our elastography method is sensitive enough to detect it. To this end, an experiment was designed containing four groups of eight spheroids each, to which different cavitation treatments were applied. The spheroids were initially all identical (composed of 30 000 cells, 2/3 of iMEF and 1/3 of KPC). There were three groups undergoing cavitation treatment with three different cavitation conditions: 20-20, 26-20 and 26-60 (the first number being the cavitation level in dB and the second number the treatment time in seconds), and one control group. Figure 9a shows the results of the statistical study carried out for this experiment, comparing first the mean wave velocities before/after cavitation treatment for each spheroid. This difference is non-significant (ns) for the control group ($p>0.999$) and significant for each of the three cavitation groups. Hence, whatever the cavitation conditions, the treatment induced a significant softening of the tumor pattern. This confirms the result previously obtained under nominal conditions. Next, the groups were compared between each other. What can be deduced from figure 9b is that there is no significant difference between the several treated groups after treatment.

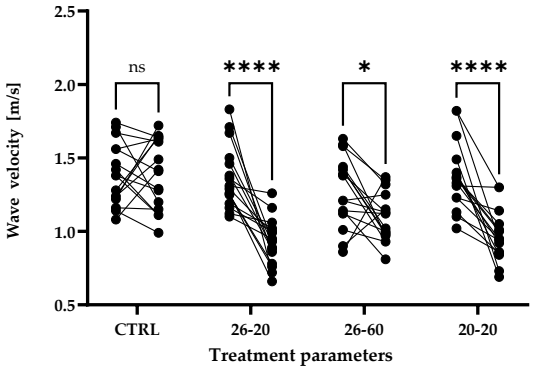

(a) Comparison before/after

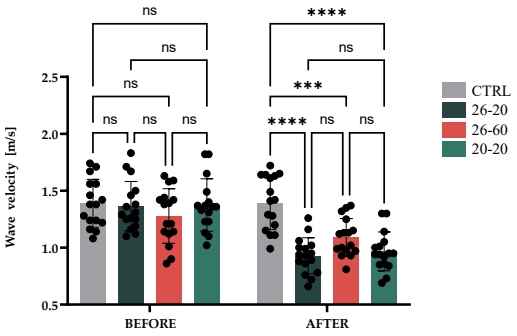

(b) Comparison between groups

Figure 9: Statistical analysis of the results of the experiment comparing groups undergoing cavitation treatments with different parameters.

Influence of the spheroids composition Finally, the influence of spheroid composition was studied. The total number of cells constituting the spheroid was kept constant but the proportion of fibroblasts and cancer cells was varied. The proportion of iMEF fibroblasts, initially set at 2/3 to mimic the composition of a real pancreatic tumor, was varied between 1/3 and 2/3. This experiment consisted of 4 groups of 8 spheroids: a control group with 2/3 iMEF spheroids undergoing no cavitation treatment, then three

groups containing respectively 1/3, 1/2 and 2/3 of fibroblasts undergoing cavitation treatment with parameters 26-20. The results of statistical tests for this experiment are presented in figure 10. First, the difference between before and after treatment is studied. As before, this difference was not statistically significant for the control group (p=0.212), but was significant for the 1/3 and 1/2 groups ($p<0.001$ and $p<0.01$, respectively). On the other hand, the p-value was 0.09 for the 2/3 group, which is not considered to be significant. It is observed that the p-value increases with the concentration of iMEF inside the spheroid, hence the difference is less significant when there are more fibroblasts inside the spheroid.

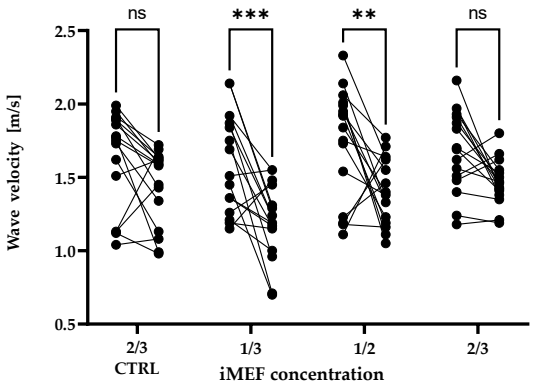

(a) Comparison before/after

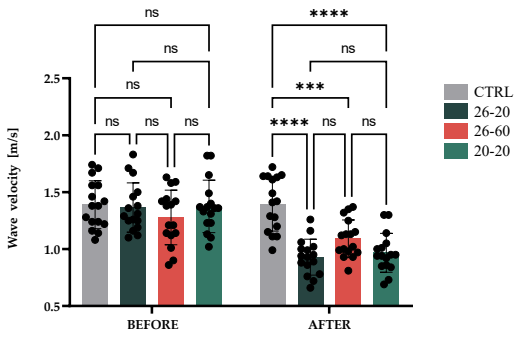

(b) Comparison between groups

Figure 10: Statistical analysis of the results of the experiment comparing groups of spheroids having different compositions but undergoing the same cavitation treatment.

The next step is to compare the different groups to determine whether the measurement is sensitive to differences in the spheroid composition. Firstly, before treatment, there is no significant difference between the groups, which means that the spheroids all have similar mechanical properties. After cavitation treatment, the only statistically significant difference was between the 1/3 spheroid group and the 2/3 group. In addition, the average velocity after treatment increased as the proportion of fibroblasts increased. This result suggests that the fewer fibroblasts there are in the spheroid, the lower the mean wave velocity is after treatment, or the more sensitive the spheroid is to cavitation.

Discussion

The results exposed in this work showed that a magnetic pulse applied onto magnetic tumor models allows to generate elastic waves, whose velocity was measured and allowed to investigate the mechanical effect of a cavitation treatment.

For this study, an original wave source has been used, consisting in applying a magnetic pulse onto samples containing magnetic nanoparticles. This is a first important result: shear waves could be generated by applying a magnetic pulse on tumor models containing magnetic nanoparticles. In micro-elastography, using oscillating micro-pipettes to generate shear waves within cells [23] has some limitations. Indeed, it leads to artifacts in the vicinity of the pipette and the velocity measurement is performed on a cell that is pre-stressed by the slight suction of the pipette, which undoubtedly has an influence on its mechanical properties. Hence, this contact-less source is of high interest for micro-elastography experiments.

In addition, the wave velocities that were measured inside the spheroids were in agreement with the values of shear wave velocities in biological tissues and more particularly in cells [23]. However, by considering the ratio between the wavelengths (around $500\,\mu m$) and the sample size (approximately 700-800 μm), there is a good chance that the waves observed here were not volumetric shear waves but guided waves. Indeed, since the wave-

lengths were not very small compared to the sample size, the waves were sensitive to the boundaries and guided by the sample geometry [24]. This is why the wave speed measurements could not be converted in elasticity values easily. To counteract this effect, the use of higher-frequency waves would reduce the wavelengths size and allow to get proper volume shear waves. In addition, this scale change could make it possible to be sensitive to the intrinsic elasticity of cells rather than to the rigidity of inter-cellular bonds. This would involve varying the type of magnetic excitation, in particular the pulse duration, in order to generate other frequency ranges within the spheroid.

When considering the wave velocity maps that were obtained, the same spatial distribution was observed in all cases: a outer region which exhibits a higher wave velocity than the center. Even if it is difficult to assess whether it is a boundary effect or a real feature, this observation is possibly compatible with the existence of a necrotic core within the spheroid that could be softer than the exterior. Measurements conducted using Brillouin light scattering on spheroids [11], while not giving absolute elasticity values either, do provide maps comparing relative elasticity between different zones of the spheroid. They also observed a higher elasticity near the surface of the spheroid, which is therefore compatible with our observations made by elastography.

Moreover, an object like a spheroid is certainly not fully described by two elastic moduli solely as an elastic, homogeneous, isotropic and linear medium. Indeed, it is a compact cellular cluster, but microscopic observation reveals discontinuities. If we consider a spheroid as a stack of incompressible spheres, the inter-cellular spaces are occupied by a fluid. Following this description, the spheroid could be considered as a discontinuous medium, or possibly as a porous medium made up of two phases, solid and liquid. Thus, even without considering the guidance effects, the physical sense of such a wave velocity measurement is hard to determine. Indeed, depending on the ratio of wavelength to spheroid and cell sizes, the waves are not sensitive to the same elastic modulus, whether they "feel" or not the evoked discontinuities.

Last, it should be noted that there is a high variability in the wave velocity measurement on the spheroids. For example, before the cavitation treatment, the value can vary by a factor of 2 between different spheroids. But since there is no reference method for this kind of measurement, it is hard to assess whether this variability comes from the measurement method or the spheroid model. Anyhow, even when spheroids are manufactured according to a
strictly reproducible protocol, they are not all the same. This great variability between spheroids explains why statistical studies were necessary to get significant and reliable results. In addition, even when performing statistical analysis on the measurements, two inconsistent results were shown in this paper: applying a cavitation treatment of 26-20 on spheroids containing 2/3 of fibroblasts led to a statistically significant difference in wave velocities in figure 9 but to a non-significant difference in figure 10. These two results were inconsistent, but when stitching both measurements, a significant result was obtained (see figure 8). It should be noted here that the result obtained regarding the cavitation effect as a function of the spheroid composition can could be highly valuable in the context of further development of such a treatment. Indeed, it could mean that the more stroma there is within the tumor, the more difficult it is to soften it using cavitation, or the less efficient the ultrasonic treatment is.

CONCLUSION

In conclusion, an original micro-elastography method has been described consisting in using a magnetic pulse applied onto magnetic spheroids. It enables to generate elastic waves within a tumor model and to assess its elasticity by measuring the average wave velocity. It was shown statistically that cavitation treatment significantly altered the wave velocity within the spheroids, indicating that the treatment resulted in a tumor softening. Since it is now well known that the mechanical constraints and elasticity play an important role in tumor growth, it is of high interest to characterize me-

chanically this type of biological samples.

ACKNOWLEDGMENTS

The authors sincerely thank Soufiane Belabhar for his technical support for the experimental setup design. They also thank Julie Guillermet-Guibert from Centre de Recherche en Cancérologie de Toulouse for providing us with the KPC and iMEF cells.
This work was partly funded by the French National Agency for Research (Investissements d'avenir ANR-10-LABX-0061) and received financial support from ITMO Cancer of Aviesan on funds administered by INSERM.

APPENDIX A: MORPHOLOGY OF THE SPHEROIDS DURING THEIR FORMATION

The evolution of the morphology of the spheroids during their formation is illustrated in Fig.11.

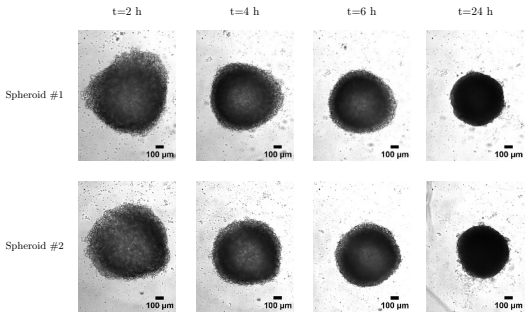

Figure 11: Microscopic images of two spheroids during their formation.

APPENDIX B: EXPERIMENTS ON GELATIN PHANTOMS

Prior to applying the magnetic pulse technique onto biological samples, experiments were carried out on phantoms in order to get a proof-of-concept of this original technique. The experimental setup, consisting in an optical microscope, an ultrafast camera, a magnetic pulse generator and a gelatin phantom containing magnetic nanoparticles is presented in figure 12a. An optical image of the magnetic phantom obtained with the optical microscope is shown in figure 12b.

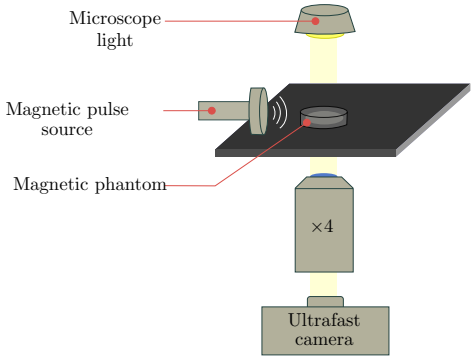

(a) Experimental setup.

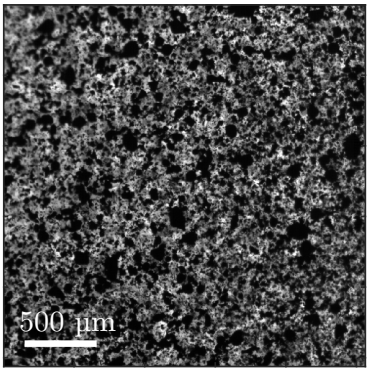

(b) Microscope image.

Figure 12: Experimental setup used for microelastography experiments on magnetic phantoms. (a) Scheme of the experimental setup. (b) Optical image acquired by the microscope ($\times 4$ lens) of a gelatin phantom containing magnetic nanoparticles.

From the ultrafast optical video, the particle velocity wavefield is retrieved using Particle Imaging Velocimetry algorithms. Two sequences of five successive snapshots are displayed in figure 13. The varying waveform and propagation direction show that the magnetic pulse applied onto a magnetic phantom allowed to generate a diffuse elastic wave field. The signal is represented as a function of time on figure 13b and its spectrum is displayed on figure 13c.

Finally, noise correlation algorithms were ap-

plied to this diffuse wave-field and a wave velocity of $3.75 \pm 0.8\ m/s$ is obtained. This value is compatible with other measurements obtained using shear wave elastography on gelatin phantoms [24, 25].

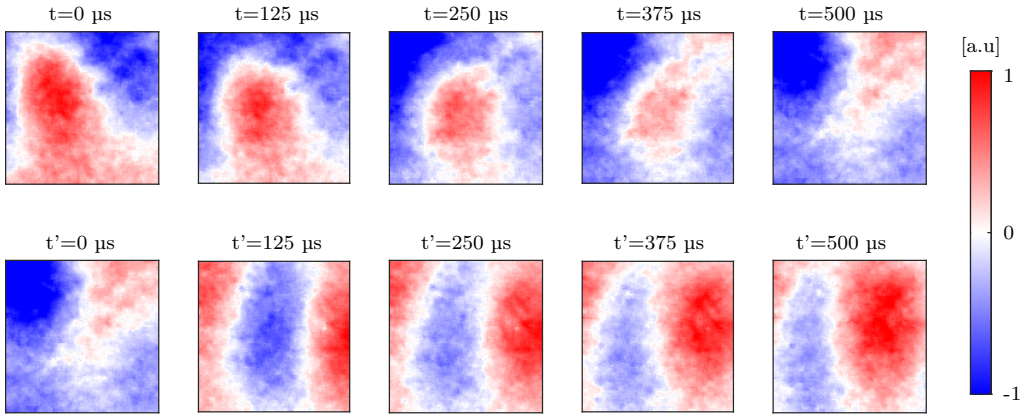

(a) Particle velocity field

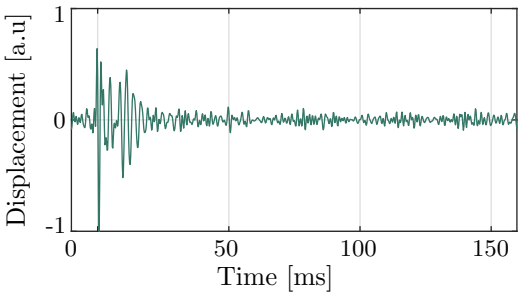

(b) Temporal signal.

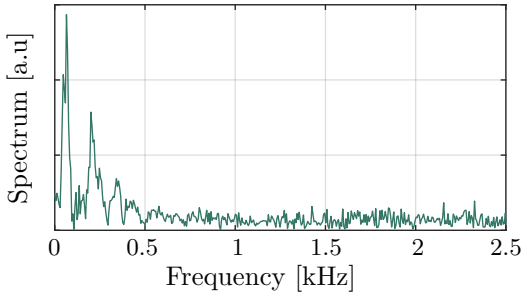

(c) Spectrum.

Figure 13: Particle velocity field acquired in a 10% homogeneous gelatin phantom. Two series of five successive snapshots are displayed, showing that the wavefront shape and the propagation direction vary along time. Hence the magnetic pulse allows to create a diffuse elastic wave field.

REFERENCES

[1] *Global Cancer Observatory*, https://gco.iarc.fr/.

[2] L. Rahib, B. D. Smith, R. Aizenberg, A. B. Rosenzweig, J. M. Fleshman, and L. M. Matrisian, Projecting Cancer Incidence and Deaths to 2030: The Unexpected Burden of Thyroid, Liver, and Pancreas Cancers in the United States, Cancer Res. **74**, 2913–2921 (2014).

[3] K. Spanknebel and K. C. Conlon, Advances in the surgical management of pancreatic cancer, Cancer J. (Sudbury, Mass.) **7**, 312–323 (2001).

[4] B. Farran and G. P. Nagaraju, The dynamic interactions between the stroma, pancreatic stellate cells and pancreatic tumor development: Novel therapeutic targets, Cytokine & Growth Factor Rev. **48**, 11–23 (2019).

[5] H. J. Jang, J.-Y. Lee, D.-H. Lee, W.-H. Kim, and J. H. Hwang, Current and Future Clinical Applications of High-Intensity Focused Ultrasound (HIFU) for Pancreatic Cancer, Gut Liver **4**, S57 (2010).

[6] T. Li, Y.-N. Wang, T. D. Khokhlova, S. D'Andrea, F. Starr, H. Chen, J. S. McCune, L. J. Risler, A. Mashadi-Hossein, S. R. Hingorani, et al., Pulsed High-Intensity Focused Ultrasound Enhances Delivery of Doxorubicin in a Preclinical Model of Pancreatic Cancer, Cancer Res. **75**, 3738–3746 (2015).

[7] R. Leenhardt, M. Camus, J. L. Mestas, M. Jeljeli, E. Abou Ali, S. Chouzenoux, B. Bordacahar, C. Nicco, F. Batteux, C. Lafon, et al., Ultrasound-induced Cavitation enhances the efficacy of Chemotherapy in a 3D Model of Pancreatic Ductal Adenocarcinoma with its microenvironment, Sci. Reports **9**, 18916 (2019).

[8] C.-E. Leroux, J. Palmier, A. C. Boccara, G. Cappello, and S. Monnier, Elastography of multicellular aggregates submitted to osmo-mechanical stress, New J. Phys. **17**, 073035 (2015).

[9] D. Jaiswal, N. Cowley, Z. Bian, G. Zheng, K. P. Claffey, and K. Hoshino, Stiffness analysis of 3D spheroids using microtweezers, PLOS ONE **12**, edited by E. Dague, e0188346 (2017).

[10] Y. Abidine, A. Giannetti, J. Revilloud, V. M. Laurent, and C. Verdier, Viscoelastic Properties in Cancer: From Cells to Spheroids, Cells **10**, 1704 (2021).

[11] J. Margueritat, A. Virgone-Carlotta, S. Monnier, H. Delanoë-Ayari, H. C. Mertani, A. Berthelot, Q. Martinet, X. Dagany, C. Rivière, J.-P. Rieu, et al., High-Frequency Mechanical Properties of Tumors Measured by Brillouin Light Scattering, Phys. Rev. Lett. **122**, 018101 (2019).

[12] J. H. Mason, L. Luo, Y. Reinwald, M. Taffetani, A. Hallas-Potts, C. S. Herrington, V. Srsen, C.-J. Lin, I. A. Barroso, Z. Zhang, et al., Remote spatially variant debiased profiling of cell and tissue mechanical properties, preprint, `10.1101/2021.05.12.443111` (2021).

[13] W. Thielicke and R. Sonntag, Particle Image Velocimetry for MATLAB: Accuracy and enhanced algorithms in PIVlab, J. Open Res. Softw. **9**, 12 (2021).

[14] T. Gallot, S. Catheline, P. Roux, J. Brum, N. Benech, and C. Negreira, Passive Elastography: Shear-Wave Tomography From Physiological-Noise Correlation in Soft Tissues, IEEE Transactions on Ultrason. Ferroelectr. Freq. Control. **58**, 1122–1126 (2011).

[15] N. Benech, J. Brum, S. Catheline, T. Gallot, and C. Negreira, Near-field effects in Green's function retrieval from cross-correlation of elastic fields: Experimental study with application to elastography, The J. Acoust. Soc. Am. **133**, 2755–2766 (2013).

[16] S. Catheline, R. Souchon, M. Rupin, J. Brum, A. H. Dinh, and J.-Y. Chapelon, Tomography from diffuse waves: Passive shear wave imaging using low frame rate scanners, Appl. Phys. Lett. **103**, 014101 (2013).

[17] V. Barrere, D. Melodelima, S. Catheline, and B. Giammarinaro, Imaging of Thermal Effects during High-Intensity Ultrasound Treatment in Liver by Passive Elastography: A Preliminary Feasibility in Vitro Study, Ultrasound Medicine & Biol. **46**, 1968–1977 (2020).

[18]C. C. Church, Spontaneous homogeneous nucleation, inertial cavitation and the safety of diagnostic ultrasound, Ultrasound Medicine & Biol. **28**, 1349–1364 (2002).

[19]K. Chettab, J.-L. Mestas, M. Lafond, D. E. Saadna, C. Lafon, and C. Dumontet, Doxorubicin Delivery into Tumor Cells by Stable Cavitation without Contrast Agents, Mol. Pharm. **14**, 441–447 (2017).

[20]K. Chettab, S. Roux, D. Mathé, E. Cros-Perrial, M. Lafond, C. Lafon, C. Dumontet, and J.-L. Mestas, Spatial and Temporal Control of Cavitation Allows High In Vitro Transfection Efficiency in the Absence of Transfection Reagents or Contrast Agents, PLOS ONE **10**, edited by R. V. Shohet, e0134247 (2015).

[21]M. Lafond, F. Prieur, F. Chavrier, J.-L. Mestas, and C. Lafon, Numerical study of a confocal ultrasonic setup for cavitation creation, The J. Acoust. Soc. Am. **141**, 1953–1961 (2017).

[22]C. Fant, M. Lafond, B. Rogez, I. S. Castellanos, J. Ngo, J.-L. Mestas, F. Padilla, and C. Lafon, In vitro potentiation of doxorubicin by unseeded controlled non-inertial ultrasound cavitation, Sci. Reports **9**, 15581 (2019).

[23]P. Grasland-Mongrain, A. Zorgani, S. Nakagawa, S. Bernard, L. G. Paim, G. Fitzharris, S. Catheline, and G. Cloutier, Ultrafast imaging of cell elasticity with optical microelastography, Proc. Natl. Acad. Sci. **115**, 861–866 (2018).

[24]G. Laloy-Borgna, A. Zorgani, and S. Catheline, Micro-elastography: Toward ultrasonic shear waves in soft solids, Appl. Phys. Lett. **118**, 113701 (2021).

[25]A. Zorgani, T. A. Ghafour, M. Lescanne, S. Catheline, and A. Bel-Brunon, Optical elastography: tracking surface waves with digital image correlation, Phys. Medicine Biol. **64**, 055007 (2019).